International Conference on Mathematics and Computational Methods Applied to Nuclear Science & Engineering (M&C 2013)
Sun Valley, Idaho, USA, May 5-9, 2013, on CD-ROM, American Nuclear Society, LaGrange Park, IL (2013)

TEMPERATURE-EXTRAPOLATION METHOD FOR IMPLICIT MONTE CARLO - RADIATION HYDRODYNAMICS CALCULATIONS

Ryan G. McClarren
Department of Nuclear Engineering
Texas A&M University
3133 TAMU, College Station, TX 77802
rgm@tamu.edu

Todd J. Urbatsch
XTD–5: Air Force Systems
Los Alamos National Laboratory
P.O. Box 1663, Los Alamos, NM 77845
tmonster@lanl.gov

ABSTRACT

We present a method for implementing temperature extrapolation in Implicit Monte Carlo solutions to radiation hydrodynamics problems. The method is based on a BDF-2 type integration to estimate a change in material temperature over a time step. We present results for radiation only problems in an infinite medium and for a 2-D Cartesian hohlraum problem. Additionally, radiation hydrodynamics simulations are presented for an RZ hohlraum problem and a related 3D problem. Our results indicate that improvements in noise and general behavior are possible. We present considerations for future investigations and implementations.

Key Words: radiation hydrodynamics, implicit Monte Carlo, time integration

1. INTRODUCTION

In this paper we are dealing with transport problems for thermal x-ray radiation in the context of radiation hydrodynamics. In such problems the radiation can carry a significant amount of energy relative to the internal energy of the materials. Also, the problems are nonlinear in that the emission of radiation is a function of material internal energy which is affected by the absorption and emission of radiation.

A well-known (and used) method for solving the radiation transport in these problems is the Implicit Monte Carlo (IMC) method of Fleck and Cummings [1]. This method has been around since the 1970s and it can give accurate solutions when run correctly. Nevertheless, IMC has errors, and these errors occur even in the limit of an infinite number of particles. As discussed in Densmore and Larsen [2], the error in IMC is composed of mesh errors, time discretization errors, and linearization errors. These errors can be counterintuitive, even to the most-hardened transport expert. For instance, in diffusive media, IMC can give better answers with larger mesh cells and time steps to the way the "implicit" character of the method behaves as a function of time step size.

Over the years there has been much research into improving this method (see, for example, [5–9]). This paper will detail an approach to deal with time and linearization errors. Fundamentally, though IMC has implicit in the title there are some quantities that are evaluated explicitly. In particular the blackbody source and material opacity are evaluated using the previous time step's temperature. This can lead to

errors in problems where there are rapid transients in the material temperatures. For example in the classical Marshak wave problem, the cold optically thick material in front of the wave will often behave abnormally. This is a result of the fact that the material does not "know" that during a time step it is heating up and becoming optically thin.

The idea that we explore in this work is to use the two previous time-steps temperatures to center the linearization inherent in IMC about a mid-time temperature instead of the previous time step's value. We do this based on the BDF-2 method [3] for integrating the material temperature equation. BDF-2 is a time integration method that implicitly computes a second-order update by differently differencing the time derivative operator. This also allows us to evaluate the opacity at a mid-time-step temperature. The result of this change is a method that, in terms of implementation, looks identical to IMC with a slight change to the Fleck factor, the temperatures evaluated at an average of the previous two time steps.

This work is an extension of the work presented at the 2012 ANS Winter Meeting [10]. We give thorough detailing of the behaviour of the method that was not possible in that forum. We also extend the method and test it on radiation hydrodynamics problems (i.e., where the radiation is transporting through a moving material).

2. DERIVATION OF THE METHOD

Consider a gray radiative transfer problem*, defined by an equation for the specific intensity of radiation, $\psi(r,\Omega,t)$,

$$\frac{1}{c}\frac{\partial\psi}{\partial t}+\Omega\cdot\nabla\psi+\sigma(T)\psi=\frac{\sigma(T)acT^4}{4\pi}+\frac{Q}{4\pi}, \tag{1}$$

and a temperature equation

$$\frac{\partial E_{\mathrm{m}}}{\partial t}=c\sigma(T)(E_{\mathrm{r}}-aT^4), \tag{2}$$

where $E_{\mathrm{m}}(r,t)$ is the material specific internal energy which is related to the temperature by an equation of state:

$$\frac{\partial E_{\mathrm{m}}}{\partial t}=C_{\mathrm{v}}(T)\frac{\partial T}{\partial t}.$$

Also in Eq. (2), $E_{\mathrm{r}}(r,t)$ is the radiation energy density (a quantity proportional to the zeroth angular moment of the specific intensity):

$$E_{\mathrm{r}}(r,t)=\frac{1}{c}\int_{4\pi}\psi(r,\Omega,t)\,d\Omega. \tag{3}$$

In Eq. (1) we have neglected scattering for convenience; including scattering is straightforward and does not change our method.

We wish to develop a set of linearized equations that are suitable for solution via a Monte Carlo technique. To do this we will find a means of approximating the T^4 term. First, we difference the time derivative in Eq. (2) using a backward difference formula of order 2 (the BDF-2 method) [3]. This method takes a differential equation of the form

$$\frac{du(t)}{dt}=f(u(t)),$$

*Our derivation is concerned with gray problems out of a desire for the clearest presentation of the method. The extension to multifrequency transport is completely straightforward as in standard IMC.

and integrates over a time step Δt using the formula

$$\frac{u^{n+1} - \frac{4}{3}u^n + \frac{1}{3}u^{n-1}}{\Delta t} = \frac{2}{3}f(u^{n+1}),$$

where u^n is the value of u after the n^{th} time step. This method is second-order accurate in time, provided that any nonlinearity on the right-hand side is converged, and the method is L-stable.

Applying the BDF-2 method to Eq. (2) gives

$$\frac{C_\text{v}}{\Delta t}\left(T^{n+1} - \frac{4}{3}T^n + \frac{1}{3}T^{n-1}\right) = \frac{2c}{3}\sigma\left(T^{n+1}\right)\left(E_\text{r}^{n+1} - a(T^{n+1})^4\right). \tag{4}$$

We then make the approximation that $E_\text{r}^{n+1} \approx E_\text{r}(t)$ and expand the term $\sigma\left(T^{n+1}\right)a(T^{n+1})^4$ using a Taylor series and then apply the chain rule:

$$\begin{aligned}\sigma\left(T^{n+1}\right)a(T^{n+1})^4 &= \sigma\left(T^{n+1/2}\right)a(T^{n+1/2})^4 + \frac{\Delta t}{2}\frac{\partial}{\partial t}\left[\sigma(T)\,aT^4\right]_{t=t^{n+1/2}} \\ &= \sigma\left(T^{n+1/2}\right)a(T^{n+1/2})^4 + \left(T^{n+1} - T^{n+1/2}\right)\frac{\partial}{\partial T}\left[\sigma(T)\,aT^4\right]_{T=T^{n+1/2}}.\end{aligned} \tag{5}$$

The temperature derivative term can be expanded as

$$\frac{\partial}{\partial T}\left[\sigma(T)\,aT^4\right]_{T=T^{n+1/2}} = 4a\sigma(T^{n+1/2})\left(T^{n+1/2}\right)^3 + a(T^{n+1/2})^4\left.\frac{\partial\sigma}{\partial T}\right|_{T=T^{n+1/2}}. \tag{6}$$

Next, we write

$$T^{n+1/2} = \frac{4}{3}T^n - \frac{1}{3}T^{n-1}, \tag{7}$$

and use this result in Eq. (5) to get

$$\begin{aligned}&\sigma\left(T^{n+1}\right)a(T^{n+1})^4 = \sigma\left(\frac{4}{3}T^n - \frac{1}{3}T^{n-1}\right)a\left(\frac{4}{3}T^n - \frac{1}{3}T^{n-1}\right)^4 \\ &+\left(T^{n+1} - \frac{4}{3}T^n + \frac{1}{3}T^{n-1}\right)\left(4a\sigma\left(\frac{4}{3}T^n - \frac{1}{3}T^{n-1}\right)\left(\frac{4}{3}T^n - \frac{1}{3}T^{n-1}\right)^3 + a\left(\frac{4}{3}T^n - \frac{1}{3}T^{n-1}\right)^4\left.\frac{\partial\sigma}{\partial T}\right|_{T=T^{n+1/2}}\right).\end{aligned} \tag{8}$$

Solving this equation for $\left(T^{n+1} - \frac{4}{3}T^n + \frac{1}{3}T^{n-1}\right)$ gives

$$\left(T^{n+1} - \frac{4}{3}T^n + \frac{1}{3}T^{n-1}\right) = \frac{\sigma\left(T^{n+1}\right)a(T^{n+1})^4 - \sigma\left(T^{n+1/2}\right)a(T^{n+1/2})^4}{4a\sigma\left(T^{n+1/2}\right)\left(T^{n+1/2}\right)^3 + a\left(T^{n+1/2}\right)^4\left.\frac{\partial\sigma}{\partial T}\right|_{T=T^{n+1/2}}}, \tag{9}$$

where we have used Eq. (7) for convenience. We can use Eq. (9) in the left-hand side of Eq. (4), and then solve for $(T^{n+1})^4$ to get

$$a(T^{n+1})^4 = ma\left(T^{n+1/2}\right)^4 + (1-m)E_\text{r}, \tag{10}$$

where

$$m = \frac{1}{1 + \frac{2}{3}\beta c\sigma\left(T^{n+1/2}\right)\Delta t}, \tag{11}$$

and

$$\beta = \frac{4a\left(T^{n+1/2}\right)^3}{C_\mathrm{v}} + \frac{\left(T^{n+1/2}\right)^4}{C_\mathrm{v}} \frac{d}{dT}\log(\sigma)\bigg|_{T=T^{n+1/2}}. \tag{12}$$

Then substituting Eq. (10) into the original radiation and material equations—Eqs. (1) and (2) respectively—we arrive at the system of equations

$$\frac{1}{c}\frac{\partial \psi}{\partial t} + \Omega\cdot\nabla\psi + \sigma\left(T^{n+1/2}\right)\psi = \frac{(1-m)c\,\sigma\left(T^{n+1/2}\right)E_\mathrm{r}}{4\pi} + \frac{m\,\sigma\left(T^{n+1/2}\right)ac\left(T^{n+1/2}\right)^4}{4\pi} + \frac{Q}{4\pi}, \tag{13a}$$

$$\frac{\partial E_\mathrm{m}}{\partial t} = mc\,\sigma\left(T^{n+1/2}\right)\left(E_\mathrm{r} - a\left(T^{n+1/2}\right)^4\right), \tag{13b}$$

where $T^{n+1/2}$ is defined in terms of T^n and T^{n-1} by Eq. (7). The system given in (13) contains the equations we seek to solve with a particle-based Monte Carlo method. This procedure closely follows that of standard IMC as presented by Fleck and Cummings. Equation (13a) is a time-dependent, linear transport equation with a known source: this equation can be solved using standard Monte Carlo procedures on prescribed spatial grid [1,4]. In this equation $m\sigma$ is an effective absorption cross-section for thermal radiation and $(1-m)\sigma$ is the effective scattering for thermal radiation. During the Monte Carlo solution of the radiation equation, the energy in the thermally-emitted particles is tracked and the energy in the absorbed particles is also tracked. The update to the material specific internal energy is then given in each grid cell by

$$\Delta E_\mathrm{m} = \sum_{i=0}^{\#\,\text{absorptions}} (h\nu)_i - \sum_{i=0}^{\#\,\text{emissions}} (h\nu)_i, \tag{14}$$

where $(h\nu)_i$ is the energy of the particle involved in event i.

2.1. Time-lumping

We generalize the form of m found in Eq. (11) to be

$$m = \frac{1}{1+\theta\beta c\sigma\left(T^{n+1/2}\right)\Delta t}, \tag{15}$$

where θ is a parameter between $\frac{2}{3}$ and 1. The value of $\frac{2}{3}$ gives the BDF-2 scheme as derived. Using a different value for θ adds a first-order in Δt error to the temperature update, though, as numerical experiments have bourne out, using a value of 1 gives more robust solutions. We call this approach time lumping because it resembles lumping in finite element methods where an error term is added to enhance stability.

2.2 Varying Δt

In the case where Δt is varying we need a different formula for $T^{n+1/2}$ than that given in Eq. (7). One can derive the BDF-2 method using variable step sizes and find that in this case

$$T^{n+1/2} = \left(1+\frac{\rho^2}{3}\right)T^n - \frac{\rho^2}{3}T^{n-1}, \tag{16}$$

where

$$\rho = \frac{\Delta t^n}{\Delta t^{n-1}}. \tag{17}$$

3. PROPERTIES OF THE METHOD

The above method has many similarities to the so-called Implicit Monte Carlo (IMC) method originally promulgated by Fleck and Cummings [1] and later advanced by many authors (see, for instance, Refs. [5,11,2,6–9]). In IMC the absorption/emission process during a time step is modeled by an effective scattering process in the same way as the BDF-2 based method. The IMC procedure defines an f factor, called the Fleck factor in the parlance of our times, as

$$f = \frac{1}{1 + \alpha\sigma\left(T^n\right)\hat{\beta}c\Delta t}, \tag{18}$$

with α a parameter between 0 and 1 known as the implicitness and

$$\hat{\beta} = \frac{4a\left(T^n\right)^3}{C_{\mathrm{v}}}. \tag{19}$$

Gentile [7] explored the inclusion of the derivative of the opacity in a slightly different form than above and found that including this information could lead to a more accurate method. Nevertheless, the $\hat{\beta}$ described above is the most common formulation.

3.1. Initializing the method

The BDF-2 is not self-starting, that is, it cannot be used for the very first time step of a calculation because two previous solutions are needed, and in the first time step only the initial condition is available. One approach is to use the IMC method to get a mid-step value of the temperature, and then use this mid-step temperature and the initial condition to do a full BDF-2 update.

To initialize our BDF-2 scheme we first integrate from time 0 to time $\Delta t/2$ using the IMC method:

$$\frac{1}{c}\frac{\partial\psi}{\partial t} + \Omega\cdot\nabla\psi + \sigma\left(T^0\right)\psi = \frac{(1-f)c\,\sigma\left(T^0\right)E_{\mathrm{r}}}{4\pi} + \frac{f\,\sigma\left(T^0\right)ac\left(T^0\right)^4}{4\pi} + \frac{Q}{4\pi}, \tag{20a}$$

$$\frac{\partial E_{\mathrm{m}}}{\partial t} = fc\,\sigma\left(T^0\right)\left(E_{\mathrm{r}} - a\left(T^0\right)^4\right), \tag{20b}$$

where in the calculation of f $\Delta t \to \Delta t/2$. The result of this step is values at the $1/2$ time level. This is followed with a BDF-2 step from $\Delta t/2$ to Δt:

$$\frac{1}{c}\frac{\partial\psi}{\partial t} + \Omega\cdot\nabla\psi + \sigma\left(T^{3/4}\right)\psi = \frac{(1-m)c\,\sigma\left(T^{3/4}\right)E_{\mathrm{r}}}{4\pi} + \frac{m\,\sigma\left(T^{3/4}\right)ac\left(T^{3/4}\right)^4}{4\pi} + \frac{Q}{4\pi}, \tag{21a}$$

$$\frac{\partial E_{\mathrm{m}}}{\partial t} = mc\,\sigma\left(T^{3/4}\right)\left(E_{\mathrm{r}} - a\left(T^{3/4}\right)^4\right), \tag{21b}$$

where

$$T^{3/4} = \frac{4}{3}T^{1/2} - \frac{1}{3}T^0, \tag{22}$$

$$m = \frac{1}{1 + \theta\beta c\sigma\left(T^{3/4}\right)\frac{\Delta t}{2}}, \tag{23}$$

and

$$\beta = \frac{4a\left(T^{3/4}\right)^3}{C_{\mathrm{v}}} + \frac{1}{C_{\mathrm{v}}}\frac{d}{dT}\log(\sigma)\bigg|_{T=T^{3/4}}. \tag{24}$$

The rest of the calculation proceeds using the method described in Sec. 2.

This initialization approach is in similar spirit to the trapezoidal BDF-2 (TBDF-2) method recently in vogue in deterministic transport calculations [12]. The TBDF-2 method uses a trapezoidal integration scheme to get a mid-step value and then BDF-2 to complete the step. This method has several benefits, second-order accuracy, L-stability, and it is self-starting—at the cost of requiring two solutions per time step. This type of approach could be adapted for Monte Carlo simulations of radiative transfer, and future work should investigate any benefits of this approach.

4. INFINITE MEDIUM TEST

In an infinite medium Eq. (1) can be simplified into a ODE for the radiation energy density:

$$\frac{dE_\mathrm{r}}{dt} = -c\sigma(T)\left(E_\mathrm{r} - aT^4\right) + Q. \tag{25}$$

Upon applying Eq. (10) to the emission term to Eqs. (25) and (2), one gets the system

$$\frac{dE_\mathrm{r}}{dt} = -mc\sigma\left(T^{n+1/2}\right)\left(E_\mathrm{r} - a\left(T^{n+1/2}\right)^4\right) + Q. \tag{26a}$$

$$\frac{dE_\mathrm{m}}{dt} = mc\sigma\left(T^{n+1/2}\right)\left(E_\mathrm{r} - a\left(T^{n+1/2}\right)^4\right) + Q. \tag{26b}$$

Given the value of E_r^n the exact solution to Eq. (26a) for a constant C_v at time level $n+1$ is

$$E_\mathrm{r}^{n+1} = \left(Er^n - a(T^{n+1/2})^4\right)e^{-cm\sigma\left(T^{n+1/2}\right)\Delta t} + a\left(T^{n+1/2}\right)^4 + \frac{Q(1-e^{-cm\sigma\left(T^{n+1/2}\right)\Delta t})}{cm\sigma\left(T^{n+1/2}\right)}, \tag{27}$$

this equation represents the solution the Monte Carlo procedure would obtain in the limit of an infinite number of particles. Then we integrate Eq. (26b) to get

$$T^{n+1} = T^n + \frac{\left(a\left(T^{n+1/2}\right)^4 - E_\mathrm{r}^n\right)e^{-c\Delta\mathrm{t}m\sigma\left(T^{n+1/2}\right)} - a\left(T^{n+1/2}\right)^4 + E_\mathrm{r}^n}{C_\mathrm{v}} + \frac{Q\left(c\Delta\mathrm{t}m\sigma\left(T^{n+1/2}\right) + e^{-c\Delta\mathrm{t}m\sigma\left(T^{n+1/2}\right)} - 1\right)}{cC_\mathrm{v}m\sigma\left(T^{n+1/2}\right)}. \tag{28}$$

The solutions in Eqs. (27) and (28) are valid for any treatment of $\sigma(T)$ as long as the value does not change during the time step.

The first test we will perform has $C_\mathrm{v} = 0.01$ GJ/cm^3-keV, $\sigma(T) = 100$ cm^{-1}, and an initial radiation temperature, $T_\mathrm{r} = (E_\mathrm{r}/a)^{1/4} = 0.5$ keV and an initial material temperature of $T = 0.4$ keV. This problem was first solved by Densmore and Larsen to examine the behavior of different Monte Carlo methods in the diffusion limit [2]. This test problem will isolate the effect of the BDF-2 approach on the emission term because the opacity is not temperature dependent.

The results for this problem using standard IMC and BDF-2 with two values of θ are shown in Figure 1. From these plots we see a stark contrast between the IMC and BDF-2 schemes. The IMC scheme has the

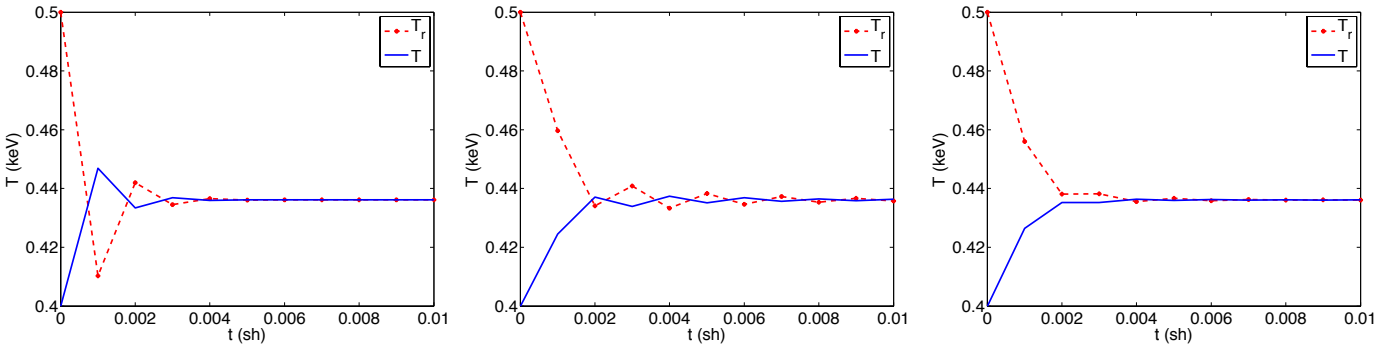

(a) IMC (b) BDF-2, $\theta = \frac{2}{3}$ (c) BDF-2, $\theta = 1$

Figure 1. Infinite medium solutions to a problem with $C_v = 0.01$ GJ/cm^3-keV, $\sigma(T) = 100$ cm^{-1}, and an initial radiation temperature, $T_r = (E_r/a)^{1/4} = 0.5$ keV and an initial material temperature of $T = 0.4$ keV. The time step size is $\Delta t = 0.001$ sh.

material temperature overshoot the radiation temperature in the first time step. This is a nonphysical result as the true solution has the radiation and material temperatures approach the equilibrium temperature monotonically. The BDF-2 results do not have the material temperature overshoot the radiation temperature in the initial time step. We do note, however, both the IMC and BDF-2 solutions have slight oscillations around the equilibrium temperature. This oscillation is more pronounced in the BDF-2 solution when $\theta = \frac{2}{3}$ compared to the solution with $\theta = 1$. We have seen similar phenomenon in a variety of test problems, and we therefore recommend using $\theta = 1$.

We can slightly modify the problem to have a larger difference between the initial material and radiation temperatures by setting the initial values as $T_r = 0.5$, and $T = 0.01$. The results from the modified problem are shown in Figure 2. For this larger difference in initial temperature, the IMC solution has the radiation temperature go well below the material temperature in the first time step. The BDF-2 solution does not have this behavior.

To add further complexity to the test problem we now allow the opacity to vary with the temperature. Specifically, we modify the problem to have $\sigma(T) = 100T^{-3}$ cm^{-1} with T in keV and increase the initial radiation temperature to $T_r = 1.0$ keV. Having temperature dependent opacities allows us to test the impact of the logarithmic derivative term in the definition of β in Eq. (12). In Figure 3 we examine the solution from standard IMC and BDF-2 with and without the logarithmic derivative term. In the standard IMC solution the material temperature goes above the initial radiation temperature. This is a violation of the maximum principle [13]. The BDF-2 solutions do not violate the maximum principle, though they do oscillate around the equilibrium temperature. These oscillations are more pronounced when the derivative of $\sigma(T)$ is included in β. We note, however, that the IMC solution does have oscillations around the equilibrium, but they are less noticeable due to the different scale in the plot.

We next turn to a problem with a temperature dependent opacity. As first posed by Gentile [7], the problem we will solve has $C_v = 0.05$ GJ/cm^3-keV, $\sigma(T) = 0.001T^{-5}$ cm^{-1} with T in keV, and an initial radiation temperature, $T_r = (E_r/a)^{1/4} = 1.465122$ keV and an initial material temperature of $T = 0.01$ keV; our solutions to this problem appear in Figure 4. This problem has an equilibrium temperature of 1 keV, though the equilibrium temperature is approached very slowly because the opacity decreases rapidly with increasing temperature—an interesting aspect of this problem is that the material emits *less* radiation as it

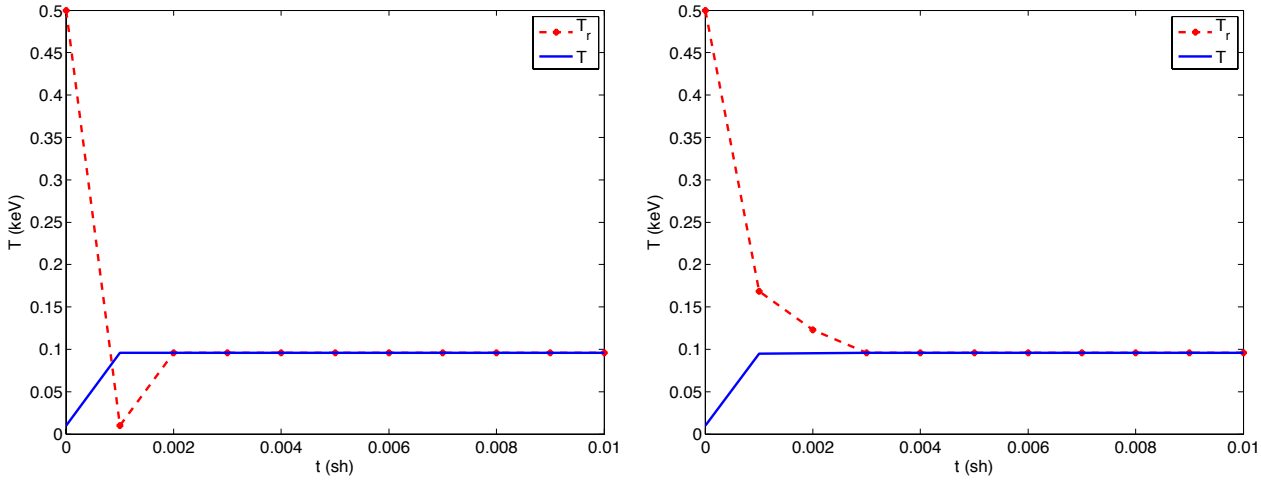

(a) IMC (b) BDF-2, $\theta = 1$

Figure 2. Infinite medium solutions to a problem with $C_\mathbf{v} = 0.01$ GJ/cm^3-keV, $\sigma(T) = 100$ cm^{-1}, and an initial radiation temperature, $T_\mathbf{r} = (E_\mathbf{r}/a)^{1/4} = 0.5$ keV and an initial material temperature of $T = 0.01$ keV. The time step size is $\Delta t = 0.001$ sh.

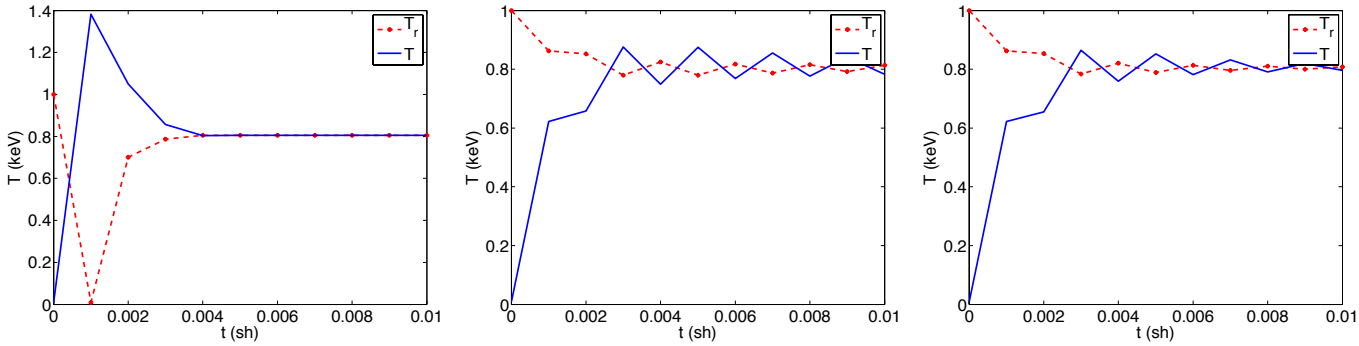

(a) IMC (b) BDF-2, $\theta = 1$, with derivative of $\sigma(T)$ term in β (c) BDF-2, $\theta = 1$, without derivative of $\sigma(T)$ term in β

Figure 3. Infinite medium solutions to a problem with $C_\mathbf{v} = 0.01$ GJ/cm^3-keV, $\sigma(T) = 100T^{-3}$ cm^{-1} with T in keV, and an initial radiation temperature, $T_\mathbf{r} = (E_\mathbf{r}/a)^{1/4} = 1.0$ keV and an initial material temperature of $T = 0.01$ keV. The time step size is $\Delta t = 0.001$ sh.

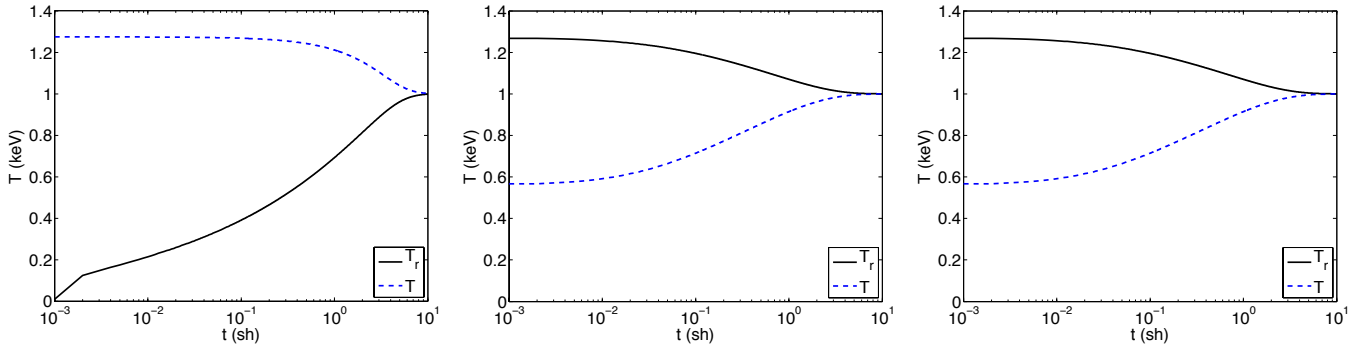

(a) IMC (b) BDF-2, $\theta = 1$, with derivative of $\sigma(T)$ term in β (c) BDF-2, $\theta = 1$, without derivative of $\sigma(T)$ term in β

Figure 4. $C_\mathbf{v} = 0.05$ **GJ/cm^3-keV,** $\sigma(T) = 0.001T^{-5}$ **cm^{-1} with** T **in keV, and an initial radiation temperature,** $T_\mathbf{r} = (E_\mathbf{r}/a)^{1/4} = 1.465122$ **keV and an initial material temperature of** $T = 0.01$ **keV. The time step size is** $\Delta t = 0.001$ **sh.**

heats up. In the IMC results (Figure 4(a)) we see a vexing phenomenon, first identified by Gentile, whereby the radiation and material temperatures "flip" in the first time step: though the initial material temperature is well below the initial radiation temperature, after the first time step the material temperature is well above the radiation temperature. The material temperature remains above the radiation temperature until equilibrium is reached. This phenomenon occurs even with very small time steps and motivated Gentile to include the derivative of the opacity in the IMC linearization. In our BDF-2 results we see that the BDF-2 solution does not have this flip of the temperatures, regardless of whether or not the derivative of the opacity is included in the simulation. Also, the behavior of the BDF-2 solutions is consistent with the analytic solution provided by Gentile in his work; the IMC solution takes much longer to reach equilibrium than the analytic solution. Therefore, we conclude that the use of the derivative of the opacity is not necessary to capture the correct behavior when using the BDF-2 method.

5. RADIATION HYDRODYNAMICS RESULTS

5.1. Implementation of a Prototype in the Cassio code

The tests so far have been radiation-only. To test the BDF-2-based extrapolation in a radiation-hydrodynamics setting, we implemented a prototype of the BDF-2-based extrapolation method in the Cassio code to test it on an ICF problem. The Cassio code is an Inertial Confinement Fusion (ICF) code in Los Alamos National Laboratory's Eulerian Applications Project. Utilizing a Godunov hydrodynamics scheme in an Eulerian frame on a unit-aspect ratio adaptive-mesh-refinement (AMR) mesh, Cassio currently has two main radiation packages for radiation-hydrodynamics simulations. It has its base diffusion capability, or it can call the Wedgehog Implicit Monte Carlo (IMC) package from the LANL's Jayenne Project [15]. The Jayenne Project IMC codes are based on the method of Fleck and Cummings [1].

Cassio uses an operator split approach where the hydrodynamics solve comes before the radiation solve withing each timestep. After the hydrodynamics solve, the temperature that is sent to the radiation package was considered to be the beginning-of-timestep temperature that we saved for the next cycle and that we used to extrapolate into the current timestep. The old temperature vector needed to be remapped to the newly refined/coarsened AMR mesh at the end of each timestep after the radiation solve. There are several

other particular items to note about this prototype:

1. We used regular IMC for the first cycle. Therefore, this prototype could not solve Gentile's equilibration problem. Normal Cassio usage starts with a small timestep size and ramps up, so this limitation should not be an issue with source-driven ICF problems that start near equilibration.
2. The emission and opacity were evaluated at the extrapolated temperature, but the heat capacity was not. This heat capacity is what is used in the calculation of the Fleck factor in the Wedgehog IMC package, not the heat capacity used to update the material state after the IMC package returns its net energy deposition.
3. No opacity derivatives were considered.
4. We used time lumping, setting the implicitness to 1.0
5. The extrapolated temperature was optionally limited to some fraction of the beginning-of-timestep temperature. Considerations were 20%, 100%, and no ceiling along with a cold floor to avoid negativities.
6. The old temperature vector was not advected with the hydrodynamics step.

The timestep control in Cassio considers many different constraints and selects the minimum value. One timestep control is some fraction of the Courant timestep limit. Another one of the controls is a velocity constraint that limits the timestep to keep material from moving more than some fraction of a cell width. Thus, a refined mesh anywhere in the problem reduces the timestep. The implication is that this BDF-2-based extrapolation will become relatively less necessary and effective as a given mesh is refined. If there were no detriment to the hydrodynamics, loosening both of these cell-size-based timestep controls could result in the BDF-2-based extrapolation showing more benefit, but then any errors from not advecting the old temperature vector could become larger.

We used a few different source biasing models in this problem. These source bias models are simple in that they merely adjust unbiasedly the numbers and weights of emission, surface source, and census particles at the beginning of each timestep according to a user supplied model. The Jayenne Project IMC algorithm nominally attempts, without source biasing, to give the same energy-weight to each particle in the problem. That means that small energy, or small volume, cells can be undersampled. With a $1/r^n$ source bias model, we can put more particles near the z-axis in RZ geometry to avoid propagating an undersampling error through the radiation-hydrodynamics algorithms. Once a source bias is used, the particles' energy-weights are not uniform across the problem, such that, especially in thin material, high-weight particles can transport across several cells in a single timestep to a region with much lower-weight particles. Splitting and Russian roulette, which have not been implemented yet, would alleviate this problem.

5.2. Hohlraum Problem in Cassio

We used the Cassio BDF-2 prototype on a problem that was based on an earlier adaptation [5] of Brunner's radiation-only ICF-like test problem [14]. In RZ geometry, a hohlraum is constructed, as shown in Fig. 5, with 0.05cm thickness, with an outer radius of 0.65cm and 1.3cm long. A block at the center of the hohlraum's interior is 0.45cm in radius and 0.4cm long. At one end, the hohlraum has an annular opening

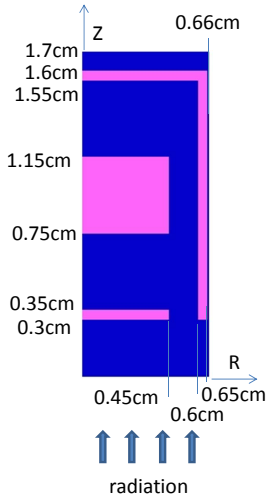

Figure 5. Schematic of a hohlraum rad-hydro test problem in RZ.

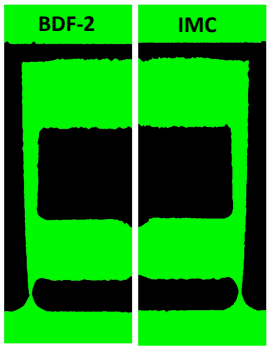

Figure 6. Material locations at 1ns. Black is aluminum, green is CH.

from 0.45cm to 0.6cm radius. A constant Planckian Blackbody surface is applied on one end of the problem, 0.3cm away from the end with the annular opening.

The Cassio hohlraum problem had an Aluminum wall and block at 2.7 g/cc and, everywhere else, Carbon-Hydrogen at a density of 1.0e-4 g/cc, all with an initial temperature of 1 eV. The drive for this problem was 400 eV. We used a multigroup opacity treatment with 102 logarithmically spaced opacity groups. Ramping linearly in time from 1e5 particles to 1e6 particles over about a nanosecond, a $[R_{\texttt{outer}}/r]^2$ source bias model was applied over each cell in the entire problem. Results at 1 ns show that the BDF-2 extrapolation was somewhat smoother. Figure 6 is a material plot that shows the Al as black and the CH as green, and that the interface appears to be slightly smoother for the BDF2-based extrapolation. A closeup of the sourced side of the hohlraum in Fig. 7 shows the regular IMC displaying more noise in the thin CH, although the BDF2-base extrapolation seems to have more axis effects inside the hohlraum. Figure 8 shows the material temperature being smoother on the Al surface in the back corner. Figure 9 shows that the BDF-2-based extrapolation gave larger timesteps for a large portion of the runtime, such that the IMC took 495 cycles and the BDF-2 396 cycles to reach 1.0 ns, requiring about 26 minutes and 22 minutes, respectively, on 32 processors of LANL's Tri-Lab Computing Cluster, Moonlight, an Opteron+GPGPU architecture from Appro.

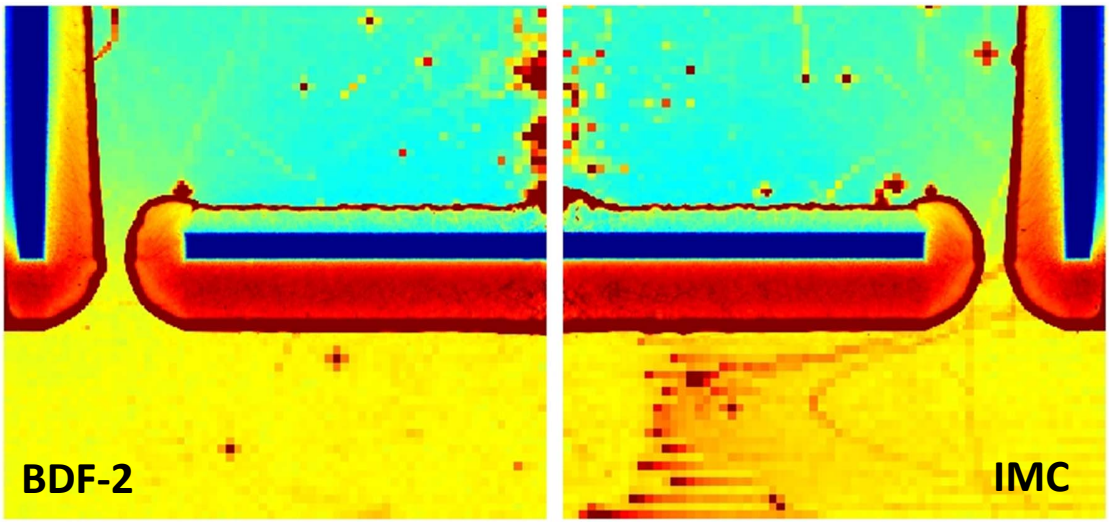

Figure 7. Near the radiation source at 1.0ns, the CH has less noise in the BDF-2-based prototype than in IMC.

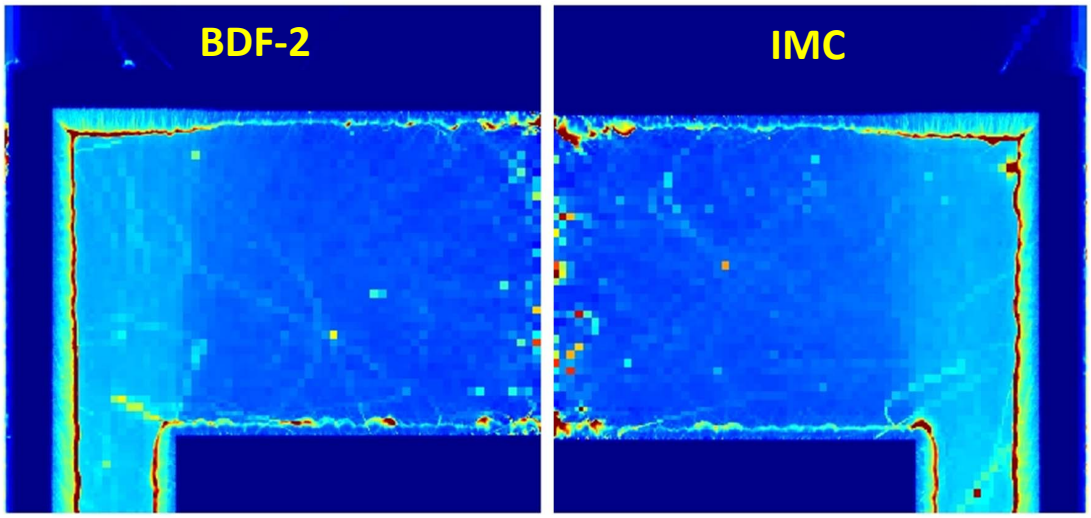

Figure 8. In the back corner of the hohlraum at 1.0ns, the BDF-2-based prototype appears to have less noise than in IMC.

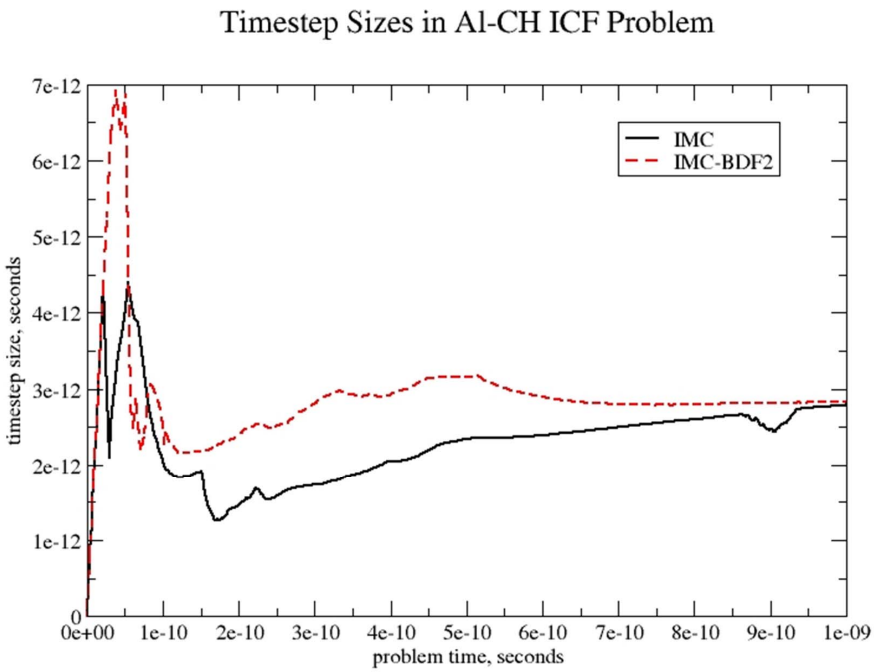

Figure 9. Longer timesteps are possible with the BDF-2-based prototype, given the same timestep constraints.

5.3. 1D Wall Problem in 3D

We next define a subset of the hohlraum problem, a 1D slab problem of 400-eV Planckian radiation traveling through 0.1cm of CH at density 1.0e-3 g/cc and impinging on a 0.02cm-thick aluminum wall. With a zeroth-level mesh of 0.01cm cubed, we looked at 4, 6, and 8 levels of refinement at the material interface, which translates to cell widths of 0.00125 cm, 0.0003125 cm, and 0.000078125 cm, respectively. Whereas the various refinement levels significantly affected the behavior of the simulation, the BDF-2 prototype appeared to have little impact on the solution. Fig. 10 shows, at the top, a close-up side view of the material temperature for the 8-levels-of-refinement problem at 0.0132ns. Both the IMC and BDF-2-based prototype look nearly the same, regardless of whether the extrapolation was limited to be within 20% of the current temperature or unbounded. The two lower plots in Fig. 10 are the IMC and BDF-2-prototype material temperatures at a cross-section slide perpendicular to the flow at x=0.099cm, which is 0.001cm in front of where the material interface originated. Visually scrutinizing the lower left subfigure of Fig. 10, it does seem that the BDF-2-based extrapolation has less overheated clumpiness.

5.4. Comments on the Radiation-Hydrodynamics problems

The BDF-2 prototype seemed to stabilize the behavior of the hohlraum problem where the CH density was 1.0e-4 g/cc. Other problems, namely where the density was higher, did not benefit as much. We discussed above how small AMR spatial cells can drive the timestep down such that the BDF-2-based extrapolation has a reduced effect. Even when the timestep was forced to be large, there appeared to be little BDF-2 improvement for many variation on the ICF problem. Therefore, another consideration is the material. The frequency integrated opacity of the CH was nonmonotonic for cold temperatures, having a large spike in the domain a few eV's. Once it heats up, though, the opacity drops significantly. Thus, stability due to

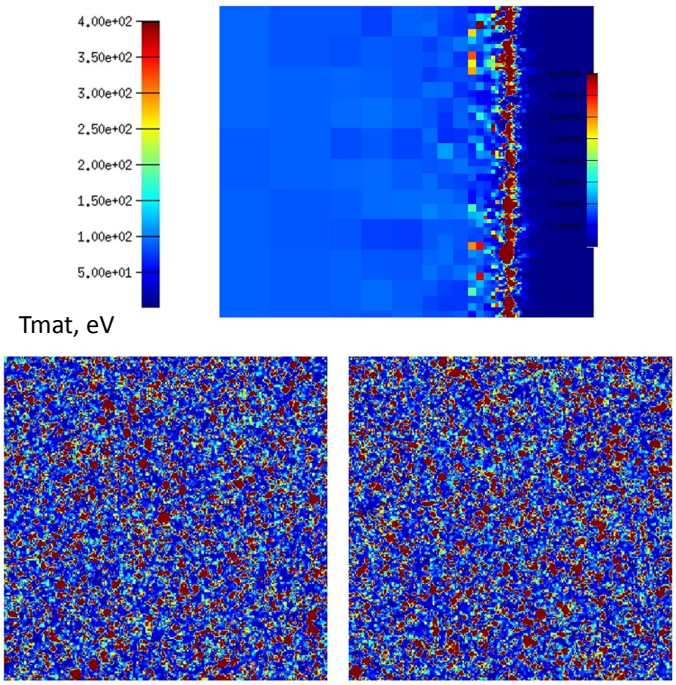

Figure 10. For a highly refined wall problem, the BDF-2 prototype had little effect. The top panel is a side view of the material temperature. The bottom left panel is a cross-sectional view at x=0.099cm, with BDF-2-based extrapolation on the left and IMC on the right.

opacity changes may not be the dominant concern here. (We did not consider any of the CH foam models that are available.) Should Cassio ever incorporate a refinement-level-dependent timestep, the BDF-2-based extrapolation could prove important for the coarser levels.

The impact of not advecting the old temperature vector each timestep needs to be investigated. It is possible that, especially for the material heterogeneities present in these ICF test problems, this is an important effect.

6. CONCLUSIONS

We have presented a new temperature extrapolation for time-Implicit Monte Carlo methods used in radiation hydrodynamics simulations. It is based on the backward difference formulation of order 2 (BDF-2) time-integration method. We have tested the method both in radiation-only and radiation-hydrodynamics simulations and shown improvements in stability.

ACKNOWLEDGMENTS

We thank Rick Rauenzahn, LANL, for pointing out the need to advect the old temperature vector in Cassio. Portions of this work were performed by Los Alamos National Laboratory under U.S. DOE contract DE-AC52-06NA25396. Release number LA-UR 13-20544.

REFERENCES

[1] J. A. Fleck, Jr. and J. D. Cummings. An implicit Monte Carlo scheme for calculating time and frequency dependent nonlinear radiation transport. *J. Comp. Phys.*, 8:313–342, 1971.

[2] J. D. Densmore and E. W. Larsen. Asymptotic equilibrium diffusion analysis of time-dependent Monte Carlo methods for gray radiative transfer. *J. Comp. Phys.*, 199:175–204, 2004.

[3] J. Stoer and R. Bulirsch. *Introduction to Numerical Analysis*. Texts in Applied Mathematics. Springer, 2002.

[4] M.H. Kalos and P.A. Whitlock. *Monte Carlo Methods*. Wiley-Blackwell, 2008.

[5] Ryan G McClarren and Todd J Urbatsch. A modified implicit Monte Carlo method for time-dependent radiative transfer with adaptive material coupling. *J. Comput. Phys.*, 228(16):5669–5686, Sep 2009.

[6] Allan B. Wollaber. *Advanced Monte Carlo Methods for Thermal Radiation Transport*. PhD thesis, University of Michigan, Ann Arbor, 2008.

[7] N. A. Gentile. A comparison of various temporal discretization schemes for infinite media radiation transport. *Trans. Am. Nuc. Soc.*, 97:544, 2007.

[8] JA Fleck and EH Canfield. A Random-Walk Procedure for Improving the Computational-Efficiency of the Implicit Monte-Carlo Method for Nonlinear Radiation Transport. *Journal of Computational Physics*, 54(3):508–523, 1984.

[9] Jesse R. Cheatham. *Truncation Analysis and Numerical Method Improvements for the Thermal Radiative Transfer Equations.* PhD thesis, University of Michigan, 2010.

[10] Ryan G. McClarren and Todd J. Urbatsch. An Implicit Monte Carlo Method Based on BDF-2 Time Integration for Simulating Nonlinear Radiative Transfer. Transactions of the American Nuclear Society 107, 502, 2012.

[11] T. M. Evans and J. D. Densmore. Methods for coupling radiation, ion, and electron energies in grey implicit Monte Carlo. *J. Comput. Phys.*, 225(2):1695–1720, 2007.

[12] Jarrod D. Edwards, Jim E. Morel, and Dana A. Knoll. Nonlinear variants of the TR/BDF2 method for thermal radiative diffusion. *Journal of Computational Physics*, 230(4):1198–1214, 2011.

[13] Edward W. Larsen and Bertrand Mercier. Analysis of Monte Carlo method for nonlinear radiative transfer. *J. Comput. Phys.*, 71:50 – 64, 1987.

[14] Brunner, T. A. Forms of approximate radiation transport. SAND2002-1778, Sandia National Laboratory, 2002.

[15] Todd J. Urbatsch and Thomas M. Evans. Milagro Version 2, An Implicit Monte Carlo Code for Thermal Radiative Transfer: Capabilities, Development, and Usage. Los Alamos National Laboratory Technical Report, LA-14195-MS, available through http://www.osti.gov, January 2005.